ELSEVIER

Wave Motion 37 (2003) 1–16

WAVE MOTION

www.elsevier.com/locate/wavemoti

# Comparison between experimental results and theoretical predictions for P-wave velocity and attenuation at ultrasonic frequency

M.S. Diallo [a,*,1], M. Prasad [b], E. Appel [c]

[a] *Department of Physics, Institute of Geophysics, Meteorology and Space Physics, University of Alberta, Edmonton, Alta., Canada T6G 2J1*
[b] *Geophysics Department, 397 Panama Mall, Stanford University, Stanford, CA, USA*
[c] *Geological Institute, Eberhard Karls University, Tübingen, Germany*

Received 10 April 2001; received in revised form 24 January 2002; accepted 8 February 2002

**Abstract**

Ultrasonic P- and S-wave velocities and attenuations have been estimated for two different sets of sandstone samples using the standard pulse transmission technique. Measurement on the first set of the samples from the Stubensandstein (Keuper Basin, southern Germany) were performed under natural conditions (e.g. without applying external pressure on the samples). For the second set of the samples, confining pressure, varying from 0 to 25 MPa was applied. Experimental results were compared to the velocity and attenuation prediction from the Biot/Squirt-flow (BISQ) model [Geophysics 58 (1993) 524] and from the reformulated BISQ model [Acoustic waves attenuation and velocity dispersion in fluid-filled porous media: theoretical and experimental investigations, Ph.D. Thesis, Eberhard Karls University, Tübingen, 2000]. The later model shows qualitative agreement between experimental and predicted velocity for the first set of sandstone samples. The attenuation, however, is highly underestimated by both models, for the second set of the samples, the Gassmann's velocity was calculated from measured dry P- and S-wave velocities in dry samples at different confining pressures, and was compared to the results of low-frequency velocity predicted from the models. It was expected that velocity predicted by both models converges to the Gassmann's velocity at confining pressure high enough to eliminate the Squirt-flow effect. Despite evidence (from the velocity versus confining pressure curves) of the closure of microcracks that enhance the Squirt-flow effect, the Gassmann's velocity was still much larger than the velocity predicted by the other models. Evidence of clay inclusion in the samples might be responsible for the poor resolution of attenuation in the Stubensandstein samples, and the disagreement between velocities in the second set.
© 2003 Elsevier Science B.V. All rights reserved.

*Keywords:* P- and S-wave velocities; Attenuation; Saturations; Viscosity; Permeability

## 1. Introduction

Considerable effort has been extended to understand the physics of the acoustic waves in saturated porous media. Pioneering work in this field is due to Biot [5] who proposed a theory of acoustic waves propagation in

* Corresponding author. Tel.: +1-780-492-4125; fax: +1-780-492-0714.
*E-mail address:* mdiallo@phys.ualberta.ca (M.S. Diallo).
[1] Previously at the Geological Institute, Eberhard Karls University, Tübingen, Germany.

0165-2125/03/$ – see front matter © 2003 Elsevier Science B.V. All rights reserved.
PII: S0165-2125(02)00018-5

**Nomenclature**

| | |
|---|---|
| $a$ | attenuation coefficient ($m^{-1}$) |
| $c_{ij}$ | elastic coefficient (GPa) |
| $\tilde{c}$ | solid frame stiffness tensor (Pa) |
| $e$ | dilatation of the solid skeleton (–) |
| $\tilde{e}$ | strain tensor (–) |
| $f$ | frequency (Hz) |
| $F$ | elastic coefficient (Biot's theory) (GPa) |
| $F_{sq}$ | elastic coefficient (BISQ model) (GPa) |
| $k$ | wavenumber (rad/m) |
| $K_b$ | bulk modulus of the dry (or drained) frame (GPa) |
| $K_f$ | bulk modulus of the fluid (GPa) |
| $K_m$ | bulk modulus of the matrix grain (GPa) |
| $m$ | inertia density of the grains ($kg/m^3$) |
| $P$ | pore fluid pressure (Pa) |
| $P_{av}$ | average pore fluid pressure (Pa) |
| $P_t$ | total pore fluid pressure (Pa) |
| $Q^{-1}$ | inverse of quality factor (–) |
| $R$ | Squirt-flow length (m) |
| $u$ | solid displacement vector (m) |
| $U$ | fluid displacement vector (m) |
| $v$ | phase velocity (m/s) |
| $V_p$ | P-wave velocity (m/s) |
| $V_{p0}$ | P-wave velocity at low-frequency limit (m/s) |
| $V_{p1}$ | fast P-wave velocity (m/s) |
| $V_{p2}$ | slow P-wave velocity(m/s) |
| $V_{p\infty}$ | P-wave velocity at high-frequency limit (m/s) |
| $V_s$ | shear wave velocity (m/s) |
| $V_{s0}$ | shear wave velocity low frequency limit (m/s) |
| $W$ | relative fluid/solid displacement vector (m) |

*Greek letters*

| | |
|---|---|
| $\varepsilon$ | dilatation in the fluid (–) |
| $\eta$ | viscosity (Pa s) |
| $\kappa$ | permeability (md) |
| $\mu$ | shear modulus (GPa) |
| $\nu$ | Poisson's ratio (–) |
| $\rho$ | saturated rock density ($kg/m^3$) |
| $\rho_a$ | coupling density ($kg/m^3$) |
| $\rho_f$ | fluid density ($kg/m^3$) |
| $\rho_m$ | matrix density ($kg/m^3$) |
| $\sigma_{ij}^f$ | part of the total stress bore by the pore fluid (GPa) |
| $\tilde{\sigma}$ | total stress tensor (GPa) |
| $\phi$ | porosity (%) |
| $\omega_c$ | Biot's characteristic frequency (rad/s) |

saturated porous media. In Biot's theory, the hydrodynamic interaction between the solid grains and pore fluid is separated into inertia interaction and viscous interaction. Velocity dispersion and attenuation result from the macroscopic flow, the so-called "global fluid flow effects". In most cases where Biot's theory has been recognised as an adequate model to account for attenuation and velocity dispersion refer to unconsolidated sediments [8,43] or highly permeable sediments [16]. However, several unsuccessful applications of the theory to laboratory data mainly from consolidated rocks intensified the discussion about its validity and the search for other mechanisms to explain the attenuation and velocity dispersion observed in laboratory experiments [36,42]. The theory's predictions for attenuation and dispersion are usually lower than measured values by one or two orders of magnitude [11]. Moreover, the theory's validity for frequency below 1000 Hz is still debated [18,37]. Several theories based on the local fluid flow or "Squirt-flow" model [26,29,32] were proposed to overcome the limitation of Biot's theory. However, extensive research on the subject showed that the Squirt-flow (e.g. microscale flow) approach cannot be viewed as an alternative to the global flow approach, but rather as another loss mechanism that contribute to the overall acoustic energy dissipation in a way not accounted by the Biot's theory [4,11]. Its significance is mainly controlled by the structure of the individual pores (e.g. aspect ratio). The very high dependence of Squirt-flow models on pore-scale parameters makes them unsuitable for the interpretation of experimental data from real porous media. The distribution of microscale inhomogeneities may be so variable that a single specific geometry of the individual pores, will not be enough to capture the acoustic response of the complex porous microstructure. Bourbié et al. [8] reviewed the different loss mechanisms and compared them with the results of laboratory studies. They concluded that, while the Squirt-flow mechanism appears to partially explain observed attenuation and velocity dispersion, it is not to be expected that a Squirt-flow model or global model taken separately is sophisticated enough to account for the loss mechanism given the complexity of the porous medium.

Recognising that both dissipation mechanisms mentioned above may be simultaneously at work in an actual saturated porous medium loaded by an acoustic wave [11] proposed a new theory of dynamic poroelasticity which combines the Biot's and the Squirt-flow mechanisms. This resulted in what is known as the Biot/Squirt-flow (BISQ) theory. Despite the significant improvement that may be obtained in acoustic data interpretation, the fact that the formulation of the BISQ theory entails a microstructural parameter (the Squirt-flow length), substantially reduces the ability of this theory to adequately predict observed velocity and attenuation in real rocks [18]. A further extension of this model to transversely isotropic media was developed by Parra [33]. Diallo and Appel [9] proposed a model similar to the BISQ model which is free of the microstructural parameter (Squirt-flow length), as no experimental method is yet available for its determination [13,44]. In this study we present, a comparison between experimental results and theoretical predictions of attenuation and velocity for two sets of sandstone samples are presented. The influence of clay on the experimental results is also discussed.

## 2. Theory

The principal difference between the Biot's model [5], the BISQ model [11] and the reformulated BISQ [9] is in the expression of total pore fluid pressure, $P_t$. In the Biot's theory [5], it is expressed as

$$P_t = P = -F\left(U_{xt} + \frac{\gamma}{\phi}u_{xt}\right), \tag{1}$$

where $U_{xt}$ and $u_{xt}$ are the fluid and solid displacements, respectively. The subscripts $x$ and $t$ indicate partial derivatives with respect to space and time, $\phi$ is the porosity of the rock and $\gamma = \alpha - \phi$, where $\alpha$ is a poroelastic coefficient. The constant $F$ is given by

$$F = \left(\frac{1}{\rho_f V_f^2} + \frac{1}{Q\phi}\right)^{-1}, \tag{2}$$

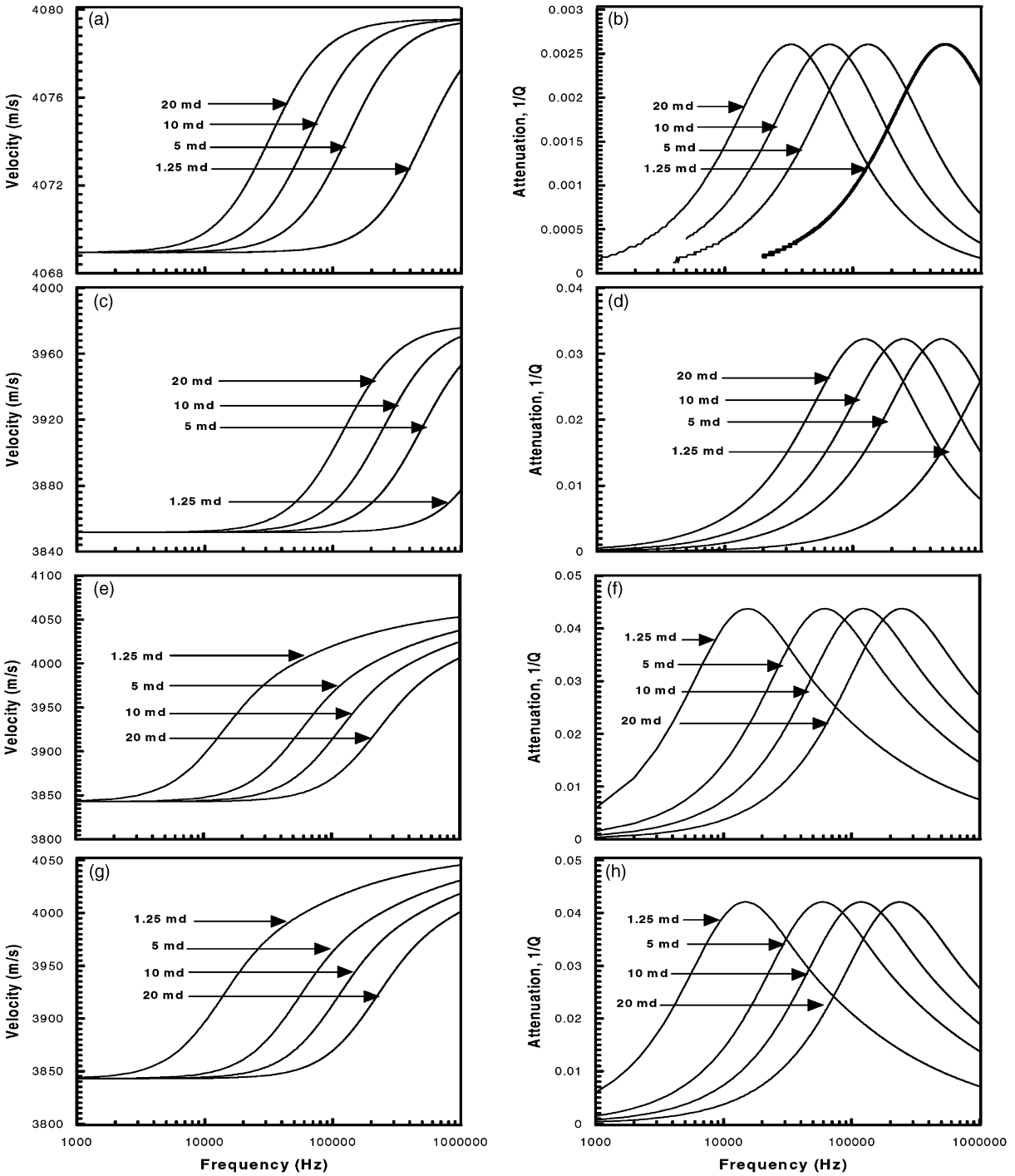


Fig. 1. Compressional velocity and attenuation variation vs. frequency for permeabilities 1.25, 5, 10 and 20 md: velocity and attenuation as predicted by ((a), (b)) Biot's theory [5], ((c), (d)) the reformulated BISQ model [9], ((e), (f)) BISQ theory [11] and ((g), (h)) extended BISQ theory to transversely isotropic media [33], after [9,10].

Table 1
Formation and saturant parameters

| Reference | Physical properties | | | | | | | |
|---|---|---|---|---|---|---|---|---|
| | $K_m$ (GPa) | $\rho_m$(kg/m$^3$) | $V_p$ (m/s) | $V_s$ (m/s) | $V_f$ (m/s) | $\rho_f$(kg/m$^3$) | $\eta$ (P) | $\phi$ (%) |
| [33] | 38 | 2650 | 3969 | 2547 | 1500 | 1000 | 0.001 | 15 |

where $\rho_f$ is the fluid density and $V_f$ is the fluid acoustic velocity. The constant $Q$ is given by

$$Q^{-1} = \frac{1}{K_m}\left(1 - \phi - \frac{K_b}{K_m}\right), \tag{3}$$

where $K_m$ and $K_b$ are the grain matrix modulus and rock bulk modulus of the rock, respectively. For the BISQ model [11], $P_t$ is given by

$$P_t = F\left[1 - \frac{2J_1(\lambda R)}{\lambda R J_0(\lambda R)}\right]\left(U_{xt} + \frac{\gamma}{\phi}u_{xt}\right), \tag{4}$$

where $R$ is the Squirt-flow length parameter, $\lambda$ the frequency-dependent parameter, and $J_0$ and $J_1$ are the Bessel function of zero and first order, respectively.

For the reformulated BISQ model [9], it is written as

$$P_t = P = -\frac{F}{\phi}(\nabla \cdot W + \alpha_0 \nabla \cdot u), \tag{5}$$

where $\alpha_0 = (\alpha + 2\phi)/3$, $W$ is the displacement of the solid frame relative to the fluid which expressed as $W = \phi(U - u)$, $P$ the pore fluid pressure, $u$ the displacement of the solid and $U$ is the displacement of the fluid.

$K_m$ and $K_b$ are the grain matrix modulus and the rock bulk modulus, respectively, $\phi$ the porosity, $V_f$ the fluid acoustic velocity and $\rho_f$ is the fluid density. Appendix A deals with the velocity and attenuation determination using the reformulated BISQ model [9]. For the other models (BISQ and Biot) details are given in [11,33]. Fig. 1 shows the effect of frequency on attenuation and phase velocity of the fast compressional wave $V_p$ by modelling the response of water-saturated porous rock for permeability values equal to 1.25, 5, 10 and 20 md with the formation and saturant parameters used in the modelling are given in Table 1.

Fig. 1 shows the difference in the frequency shift of the velocity and attenuation curves with changes in permeability between the reformulated BISQ [9] and the Biot's model [5] on the one hand and the BISQ model [11] from and its extension to transversely isotropic media [33], on the other. Considering the difference between the low-frequency and high-frequency velocity limits (which is an indicator for dispersion magnitude), the BISQ model and the reformulated BISQ model show the same order of magnitude that is much larger than that of the Biot's model [5].

## 3. Experimental procedure

### 3.1. Sample description and preparation

The rock samples used for the ultrasonic experiment are sandstones from the Stubensandstein, Keuper Basin, southern Germany. The Stubensandstein consists mainly of coarse to fine elastic arkose sandstones with clay horizons occurring between successive deposit units [20]. The permeability of the investigated samples was taken from [21] who studied quantitatively the permeability distribution in the Stubensandstein. The porosity, the grain matrix density $\rho_m$, and the sample bulk density measured using a set of Micrometerix instruments. The measurement principle is described in [20]. The petrophysical parameters of the samples are given in Table 2.

Table 2
Rock physical parameters

| Sample ID | $V_{p\,dry}$ (m/s) | $V_{p\,sat}$ (m/s) | $\rho_m$ (kg/m$^3$) | $\kappa$ (md) | $\phi$ (%) |
|---|---|---|---|---|---|
| EM50B16 | 2000 | 1940 | 2667 | 376 | 29 |
| EB36B16 | 2200 | 2230 | 2656 | 563 | 22 |

Thin sections analysis, scanning electron microscopy (SEM) and transmission electron microscopy (TEM) analysis performed by other authors (e.g. [20]), indicated that in general quartz is the predominant rock mineral (70–80%) followed by feldspars, which accounts for approximately 10–20% of the samples. The SEM analysis reveals a variety of cement types with a dominance of kaolinate and calcite. The three rock samples used for the laboratory experiment are poorly consolidated with sub-rounded, medium-sized and moderately to well sorted grains. The samples were cored to a diameter of 10 cm with length of up to 70 cm. The recovered cores were then cut into several samples of up to 10 cm length. Lengths of sample used in the experiment were further reduced to less than 4 cm to achieve a high diameter to length ratio and hence reduce the risk that onset time of the direct acoustic pulse travelling across the sample length be obscured by reflections from the sides. Because of weak cementing of the matrix grains, it was necessary to cover the sample faces with a thin viscous resin layer (epoxy) that was allowed to dry slowly under room temperature for at least 24 h to avoid deep infiltration of the viscous fluid into sample body immediately after application, which may significantly affect permeability and porosity of the samples. After the epoxy has completely hardened, the end faces were polished again to reduce the thickness of the epoxy layer, and hence, its effect on acoustic wave travel time and intrinsic attenuation.

### *3.2. Velocity measurement technique*

The fast compressional wave velocity is estimated by means of the pulse transmission (PT) technique [7,36,40] by which the travel time of the pulse across the sample was measured, and knowing the sample length, velocity was inverted. The PT module consists mainly of P-wave transducers mounted on aluminium plates. The transducers are acoustically backed by approximately 5 mm silicon layer to broaden the frequency bandwidth of the system and to attenuate the component of the P-wave emanating from the transducer's side not sitting on the aluminium plate. To prevent short-circuiting, a very fine layer of silicon was built between the transducer and the aluminium plate on which it was then screwed. The transducer on each plate was then encased in a rubber capsule with an o-ring and tightly screwed on the transmitter plate to prevent contact with the pore fluid. During the experiment, the rock sample was brought between the plates on which one transducer acting as transmitter and the other as receiver were fixed. The whole assembly was held together by a rubber sleeve. To achieve good acoustic coupling at the contact points between the sides of the aluminium plates and the sample faces (at the transmitter and receiver side), ultrasonic gel was smeared in before jacketing the assembly with the rubber sleeve. The samples were first measured dry and then wet (saturation with water) in order to measure the dry and wet (saturated) velocities. An additional measurement was performed by holding the two plates supporting the transducers head-to-head to determine the delay time in the two aluminium plates. The delay time was then subtracted from the propagation time across the sample to correct the measured velocity. After preparation, the samples were oven dried at 60 °C for several days and cooled in a tight closed glass container, shortly before measurement to avoid adsorption of moisture in the rock. Saturation was achieved by suction effect under a pressure of at least 3 bar for at least 1 week. Jaritz [21] indicated that 90% saturation degree could be achieved with this technique when samples are impregnated for at least 1 day but full saturation would require bringing the sample into a pressure vessel. The experiment was carried out under natural conditions (e.g. without exerting pressure on the sample). Apart from the PT apparatus, in which the sample was contained, the instrumental package contains additional electronics, including a digital oscilloscope, an impulse generator, and a bandpass filter. The system is controlled by a PC, using Labview II codes [30]. Fig. 2 shows the different parts of the experimental setup.

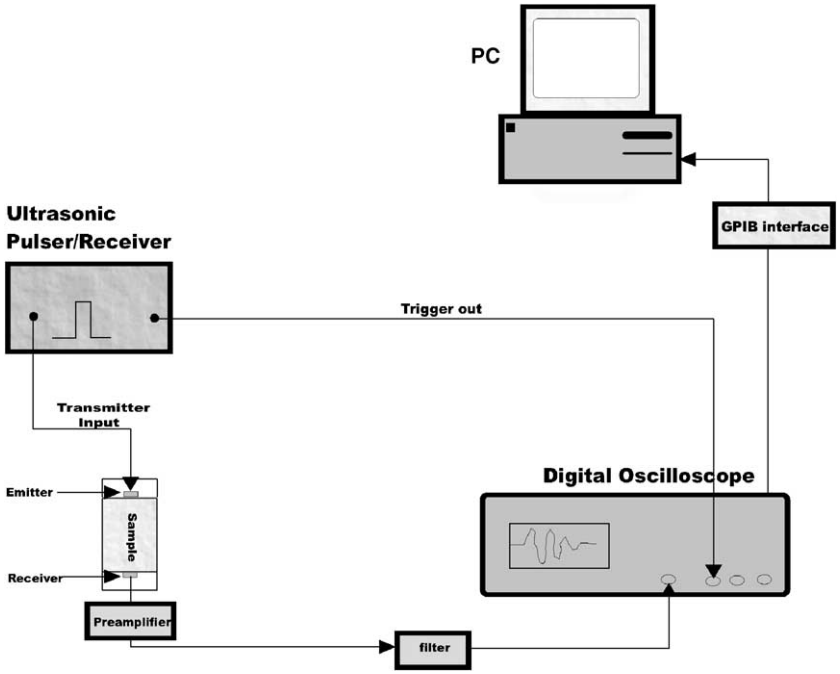


Fig. 2. Schematic drawing of the ultrasonic measurement assembly [30].

### 3.3. Attenuation determination

Anelastic attenuation is the process by which rocks convert acoustic waves into heat. The process modifies both amplitude and phase velocity of propagating waves. Basically two forms of attenuation can be distinguished depending on the mechanisms involved in the conversion of the acoustic energy into heat: extrinsic attenuation which is related to the acoustic energy loss due to, for example, spherical divergence, subsurface conditions, source geometry, etc. and intrinsic attenuation (specific attenuation) which result only from the interaction between the acoustic wave and the medium in which it propagates (e.g. porous medium) and its saturating fluids. Intrinsic attenuation can be characterised by a coefficient $a(f)$ (that depends on the frequency $f$) which defines the decrease of a sinusoidal plane wave amplitude:

$$A_x = A_0\, \mathrm{e}^{-a(f)x}, \tag{6}$$

where $A_0$ is the initial amplitude, $A_x$ the amplitude after distance $x$ and $a(f)$ is the attenuation coefficient. An alternative measure of the ability of attenuation is the specific dissipation function $Q^{-1}$, or quality factor $Q$, defined as

$$\frac{1}{Q} = \frac{\Delta E}{2\pi E}, \tag{7}$$

where $\Delta E$ is the energy dissipated per wave cycle, and $E$ is the total energy in a wave cycle. The quality factor $Q$ can be expressed in terms of the attenuation coefficient $a(f)$, phase velocity $v$ and frequency $f$ as

$$\frac{1}{Q} = \frac{a(f)v}{\pi f}. \tag{8}$$

Eq. (8) is an approximate relation that is valid either when $Q$ and $v$ are frequency independent, whereby attenuation is a linear function of frequency [22]. It is fairly well accepted that $Q$ and $a(f)$ are frequency dependent, so that

ignoring small change in the phase velocity is required to maintain linearity [24]. Even though it is the phase velocity that is involved in the expression above (Eq. (6)), in experiment with narrow bandpass (e.g. less than one decade) it is normally the group velocity that is delivered. This in turn causes an error in attenuation determination, the amount of which depends on the degree of dispersion [36]. Among the various techniques available for attenuation measurement, the most widely used are the spectral ratio [40], the rise time [15], and the pulse echo [42]. The first two techniques are usually known as *transmission techniques*, as they involve mainly the recording of an acoustic pulse which travels across the sample. Attenuation is then estimated by comparing the recorded signal propagating through the sample specimen and a reference sample with very high quality factor ($Q \approx \infty$). In the pulse echo technique, the sample is placed between tow buffer rods (usually lucite); one transducer is used, that acts as transmitter and receiver at the same time. The ultrasonic pulse travels across the buffer rod and the sample and is reflected at both ends of the sample. The two reflected pulses are recorded and then processed to obtain the magnitude and phase of each frequency. The phase difference at a given frequency is used to determine the phase velocities and the amplitudes of the reflected signals on the top and bottom of the sample; the reflection coefficient at the interface between the sample and buffer rod are used to calculate the attenuation [42]. For the spectral ratio method, usually aluminium sample (with a quality factor of about 150 000, very much higher than that of natural occurring rocks $Q \leq 1000$) is used as reference sample [40]. With the spectral ratio method, essentially two measurements are made using identical procedures: one with the rock sample of interest and the second with the reference sample (Fig. 2). Afterwards the spectral amplitudes of the recorded signal at different frequencies are compared. Because attenuation implies a preferential loss of the high frequencies, a change in the total spectrum will occur. Equations giving the spectral magnitudes of a plane seismic wave for the reference and the rock samples can be expressed as [40]

$$A_{\mathrm{ref}}(f) = G_{\mathrm{ref}}(f)\, \mathrm{e}^{-a_{\mathrm{ref}}(f)x}, \tag{9}$$

and

$$A_{\mathrm{pr}}(f) = G_{\mathrm{pr}}(f)\, \mathrm{e}^{-a_{\mathrm{pr}}(f)x}, \tag{10}$$

where $A$ is the amplitude, $f$ the frequency, $x$ the distance, $G_{\mathrm{pr}}(f)$, $G_{\mathrm{ref}}(f)$ the geometrical factors, and $a(f)$ is the frequency-dependent attenuation coefficient. The subscripts pr and ref refer to the rock probe and reference samples, respectively. Over the frequency range of 100 kHz to 1 MHz, Toksöz et al. [40] assumed that the attenuation coefficient $a(f)$ is a linear function of frequency and can be expressed as

$$a(f) = cf, \tag{11}$$

where $c$ is a constant related to the quality factor $Q$ by

$$Q = \frac{\pi}{cv}. \tag{12}$$

When the investigated sample and the reference sample have the same geometry and shape, and when similar measurement conditions are assumed (same transducers arrangement), then the factors $G_{\mathrm{pr}}$ and $G_{\mathrm{ref}}$ are frequency independent [40]. The ratio of the spectral amplitudes from the investigated and reference samples is

$$\frac{A_{\mathrm{pr}}}{A_{\mathrm{ref}}} = \frac{G_{\mathrm{pr}}}{G_{\mathrm{ref}}}\, \mathrm{e}^{-(a_{\mathrm{pr}}(f) - a_{\mathrm{ref}}(f))x}, \tag{13}$$

or

$$\ln\left(\frac{A_{\mathrm{pr}}}{A_{\mathrm{ref}}}\right) = \ln\left(\frac{G_{\mathrm{pr}}}{G_{\mathrm{ref}}}\right) + (a_{\mathrm{ref}}(f) - a_{\mathrm{pr}}(f))x. \tag{14}$$

If $Q$ of the reference sample is very high (i.e. $Q \cong \infty$), then $a_{\mathrm{ref}} = 0$. Thus, $a_{\mathrm{pr}}$ of the rock (investigated) sample can be directly determined from the slope of the linear curve expressed by Eq. (14). Knowing the velocity $v$, Eq. (12) can be finally used to obtain the quality factor or intrinsic dissipation for the investigated sample. Further details on the techniques of ultrasonic velocity and attenuation measurements are given by Thurson and Pierce [39].

## 4. Experimental results

The ultrasonic measurements were carried out on the samples described in Table 2. We observe that for the sample EM50B16, P-wave velocity for the saturated sample is lower than the dry sample. This could indicate that full saturation was not achieved. This sample offers an optimal condition to test the BISQ model, which is expected to give better results for partially saturated rocks [12]. Attenuation was determined using the spectral ratio method described earlier. Figs. 3 and 4 show power spectra from the aluminium reference samples, the rock samples and the spectral ratio, $\ln(A_{pr}/A_{ref})$. All measurements were made around 100 kHz.

The linear fitting is described by Eq. (14). Figs. 3 and 4 show predicted curves of attenuation and velocity dispersion versus frequency using BISQ [11] and the reformulated model [9]. The bulk and shear moduli were obtained by varying the Poisson's ratio within the range of 0.19–0.23 for sandstones [35], in order to obtain the best fitting between the predicted and the measured P-wave velocities. Large discrepancies between the measured and predicted velocities can still be observed. The predicted velocity obtained from the reformulated BISQ model are closer to the measured values of the velocity and attenuation. There is poor resolution in attenuation for the two samples EB36B16 and EM50B16. The shape and the geometry of the aluminium reference and rock samples are identical, and the diameter is also much larger than the thickness for both the reference and rock samples. Thus, the idea that geometrical factors such as beam spreading or reflection from the sides might be the reason for the poor

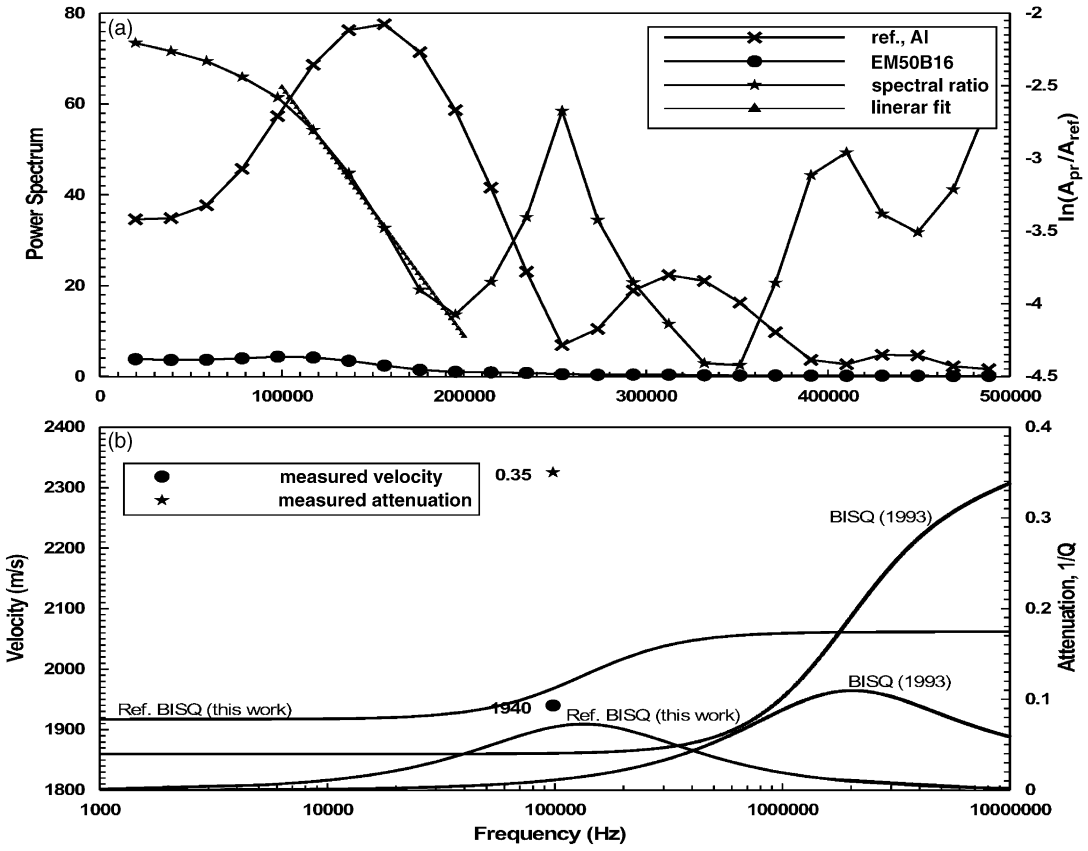


Fig. 3. (a) Power spectra from the aluminium reference sample, the rock sample (EM50B16) and the spectral ratio, $\ln(A_{pr}/A_{ref})$. (b) Compressional velocity and attenuation variation vs. frequency predicted by the reformulated BISQ model [9] and the BISQ model [11] for the sandstone sample EB36B16.

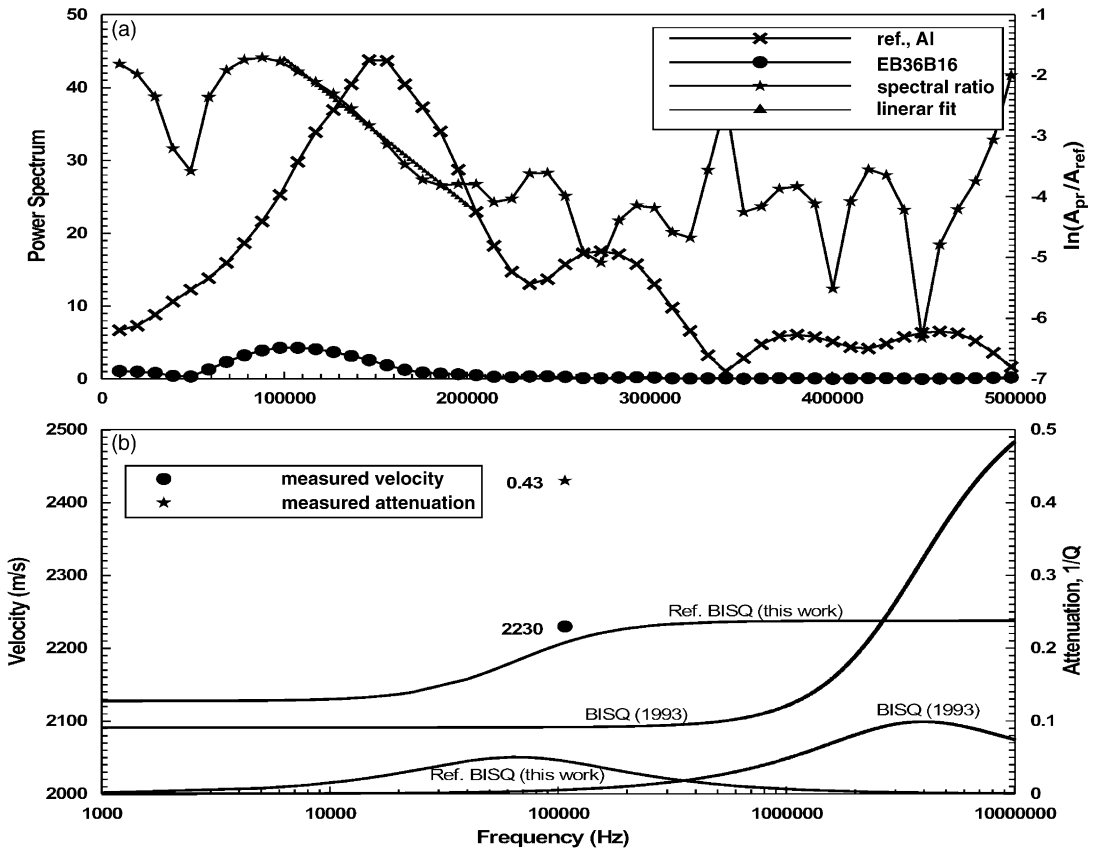


Fig. 4. (a) Power spectra from the aluminium reference sample, the rock sample (EB36B16) and the spectral ratio, $\ln(A_{pr}/A_{ref})$. (b) Compressional velocity and attenuation variation vs. frequency predicted by the reformulated BISQ model [9] and the BISQ model [11] for the sandstone sample EM50B16.

resolution in attenuation can be ruled out. Because of the assumption of partial saturation for sample EM50B16, a fairly good agreement between the measured and predicted velocity and attenuation from BISQ model [11] was expected. This being not the case it can be speculated that the models applied in this study are not adequate to explain the observed data. In this case additional interaction mechanisms other than those resulting from the global and local flow, have to be invoked unless it is considered that the poor constraint on dry rock elastic moduli is the main factor behind the misfits observed in the velocity prediction. To rule out the latter alternative (e.g. poor constraint on elastic moduli), numerical models of velocity and attenuation were computed for a sandstone sample with well known physical properties. The dry compressional and shear wave velocities were measured at different confining pressures so that the Poisson ratio, shear modulus and dry bulk modulus needed as input to the BISQ model could be determined with accuracy. The mineralogical composition is summarised in Table 3 and the physical parameters for this sample are summarised in Table 4. For this sample, the variation of the velocity and attenuation versus

Table 3
Mineralogical properties of the sandstone samples

| Sample | Quartz (%) | Plagioglas (%) | K-feldspar (%) | Clay (%) | Calcite (%) |
|---|---|---|---|---|---|
| 24 h | 68 | 27 | Trace | 4 | – |

Table 4
Physical properties of the sandstone samples

| Sample | Physical properties | | | |
|---|---|---|---|---|
| | $K_m$ (GPa) | $\rho_m$ (kg/m$^3$) | $\phi$ (%) | $\kappa$ (md) |
| 24 h | 38 | 2630 | 26.9 | 1.030 |

frequency for water saturation condition were computed at three confining pressures, using the BISQ model and the reformulated BISQ model [9]. The resulting low-frequency velocity limit at each pressure step was compared to the Gassmann velocity. With increasing confining pressure, microcracks that enhance the Squirt-flow mechanism will be gradually suppressed so that velocity dispersion can be described by the Biot's theory [26,27]. Therefore, it is expect that the low-frequency velocity limits from the BISQ model and the reformulated BISQ model should converge to the Gassmann velocity (e.g. Biot's low-frequency velocity limit) for high confining pressure. This is well illustrated by comparing the measured ultrasonic velocity and calculated velocity (Gassmann's equations) for saturated sandstone samples [14]. Similar comparison, performed for granite samples showed very good agreement between Gassmann's velocity and velocity of the saturated rock at low frequency [31]. This should be the case when no other dissipation mechanisms are at work other than that related to the Biot "global" flow or the Squirt-flow and the rock is isotropic. Fig. 5 shows predicted (calculated) results for the latter sample. The filled circles, squares and diamonds represent the calculated Gassmann velocities for the lowest, medium and highest confining pressures, respectively.

Fig. 5 shows a decrease in the difference between the Gassmann velocity and the predicted low-frequency velocity limit with increasing confining pressure for both the BISQ model and the reformulated BISQ model. At the highest confining pressure (24.8 MPa), significant discrepancies between these velocities persist. For the dry sample, P- and S-wave velocities versus confining pressure (Fig. 6), shows that beyond a pressure of 20 MPa, the velocity is almost insensitive to pressure increase. It is assumed that the velocities for the saturated samples follow the same trend. This assumption is supported by the observed variations of the saturated and dry rock velocities with respect to confining pressure from experimental data [27,45]. Klimentos [25] suggested that, at very high confining pressure where the velocity becomes insensitive to confining pressure change, open microfractures that might be still present in the rock frame have very little effect on velocity. Therefore, the assumption that the velocities for the investigated sandstone samples stabilise beyond 20 MPa, precludes any attempt to explain the difference between the Gassmann's and predicted low-frequency velocity by the Squirt-flow mechanism. However, the fact that the estimate of the low-frequency velocity is the result of the theoretical fluid substitution means that ignoring anisotropy can lead to either underestimating or overestimating the change in velocity due to fluid substitution [28]. In the present work, anisotropy was ignored as no data was available to investigate its effect. Another possible explanation could be related to the effect of the clay in the samples (Table 3). Han et al. [19] found that a small amount of clay (1–2%) can lead to a significant reduction of velocity. The effect of clay content on both P- and S-wave velocities stems mainly from the reduction it induces on the shear modulus. Wang [41] suggests that the effect of clays on seismic properties depends on the position of the clay particles in the rock and on the clay type and that except for the density effect, clay content has little effect on seismic properties unless the pore are completely filled. The latter assertion that contradicts the conlusion from [19] is an indication of how puzzling is the effect of clays on seismic properties. Despite the many attempts to explain the effect of clay content on attenuation [4,17] the mechanism by which clay content enhances attenuation is not yet fully understood. The TEM analysis conducted on several sandstone cores from the same site as the investigated samples EM50B16 and EB36B16 reveals the presence of clay appearing as disseminated intrapore growth [20] that may result form an early diagenetic transformation of feldspar. An advanced diagenetic process should normally result in similar clay particle distributions as described by Klimentos and MacCann [24] who reported significant correlation between clay content and attenuation. The expected occurrence of this type of clay in the investigated samples EM50B16 and EB36B16 could be responsible for the large discrepancy between measured and predicted attenuation values (Figs. 3–5). For the 24 h sample,

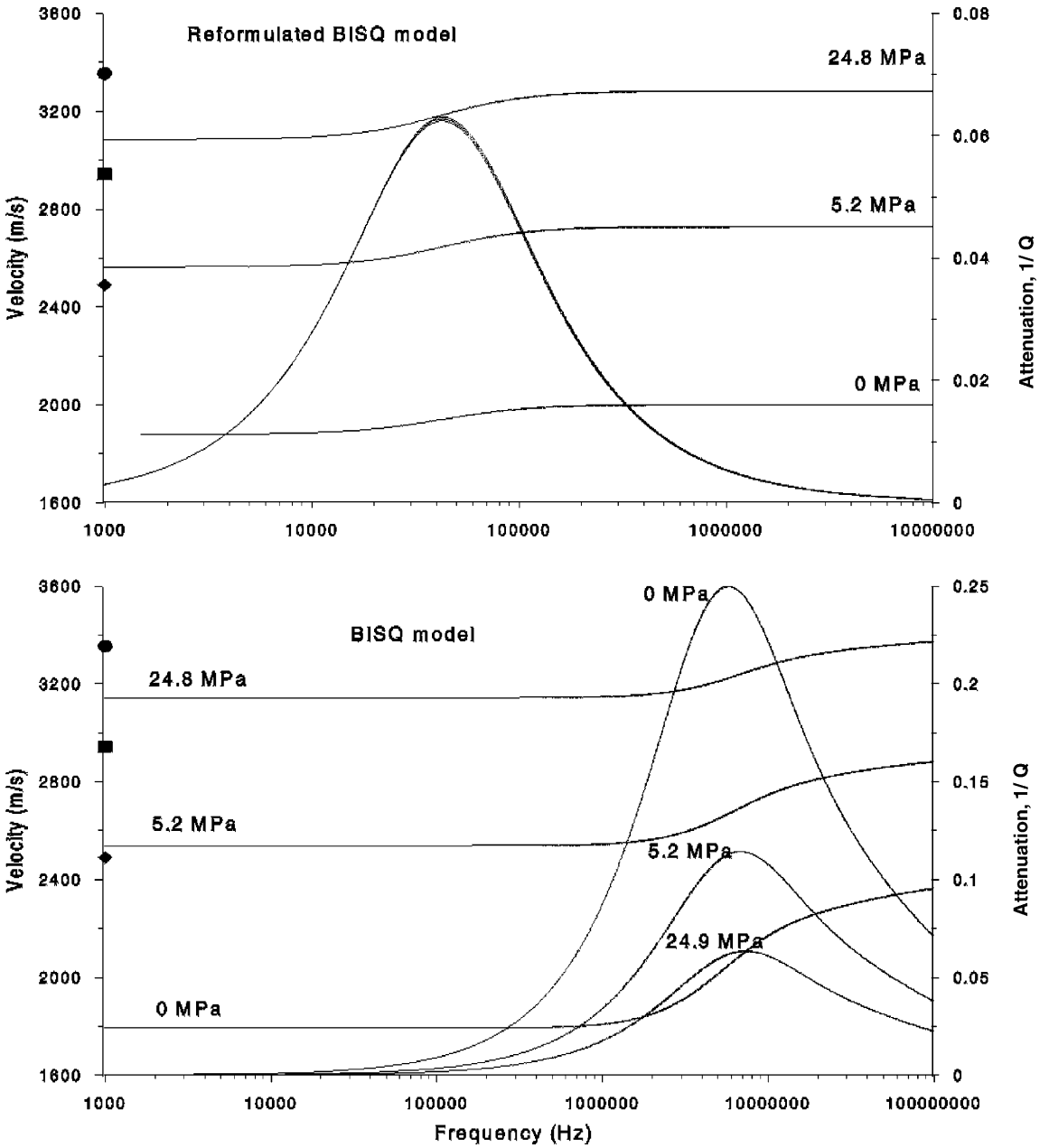


Fig. 5. Compressional velocity and attenuation variation vs. frequency for confining pressure 0, 5.2 and 24.8 MPa predicted by the reformulated BISQ model and the BISQ model for the sandstone 24 h sample. The filled circles, squares and diamonds are the Gassmann velocities at 0, 5.2 and 24.8 MPa, respectively.

attenuation data for the saturated state were not available. It is anticipated that in this case again, neither the BISQ model nor the reformulated BISQ model could provide satisfactory prediction of attenuation for this sample because of the clay effect. Attenuation curves predicted by the BISQ model are more sensitive to the increase in confining pressure than the reformulated BISQ model. The latter shows sensitivity to confining pressure increase only around

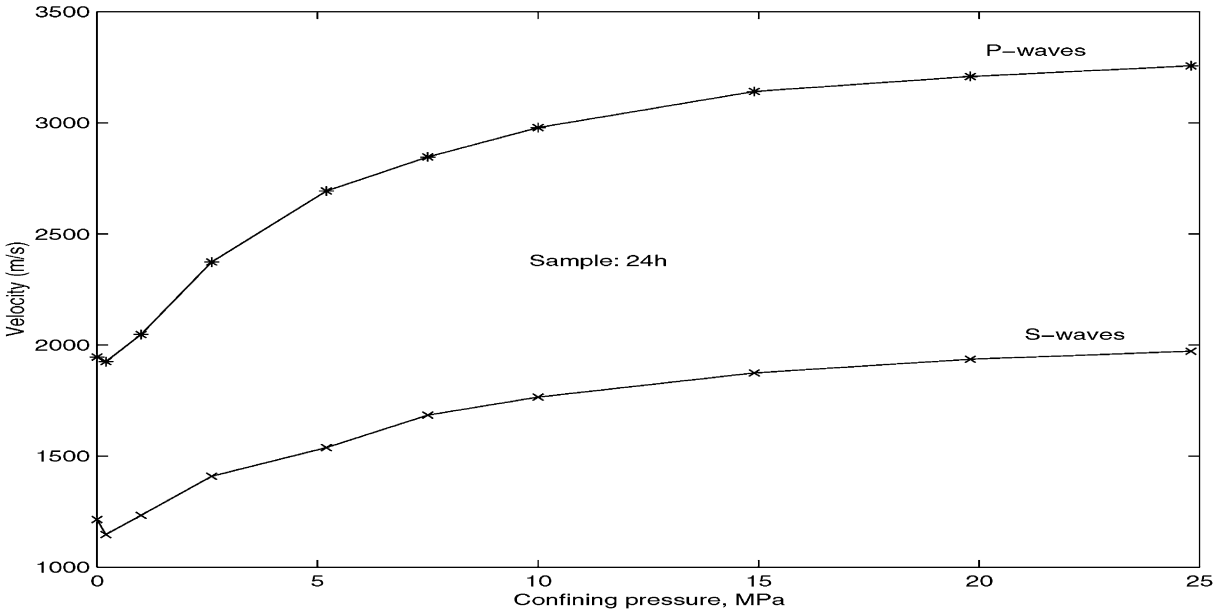


Fig. 6. Ultrasonic compressional and shear velocity variation vs. confining pressure for the dry sandstone 24 h sample (Prasad and Nur, 1999, unpublished data).

the relaxation frequency. The sensitivity remains, however, very small compared to that observed in the BISQ model curves (Fig. 5).

## 5. Conclusions

Neither the BISQ model [11] nor the reformulated BISQ model could resolve the ultrasonic data. The inadequacy of both models is best illustrated by the significant discrepancy between measured and predicted attenuation for sandstones samples from the Stubensandstein (Keuper Basin, southern Germany). Attempt to match low-frequency velocity limits to Gassmann's velocity calculated from measured compressional- and shear-waves velocities using experimental data from dry sandstone samples, was not successful either. At confining pressure which is high enough to reduce the Squirt-flow effect on velocity, a significant difference between the Gassmann's velocity and the predicted (calculated) velocity from the models was still present. It is assumed that evidence of clay inclusions in the investigated samples could be responsible for the large discrepancies in velocities and attenuations. Even though this assumption was not tested in the present work, other studies [3,17,25,38] emphasized the influence of clay inclusions in the process acoustic energy dissipation and velocity dispersion, along with the Biot's and Squirt-flow mechanism. Despite evidence of the influence of clays on velocity dispersion and attenuation, clear understanding of the process in which this occurs is not yet available. Further investigations towards that end are needed.

## Acknowledgements

This work as part of Ph.D. Thesis of the first author was supported by the Geological Institute, Eberhard Karls University, Tübingen, Germany. M. Prasad and A. Nur from the Stanford Rock Physics Group (SRB) kindly provided the data in Tables 3 and 4 for the numerical modelling. The Department of Physics, University of Alberta provided the facilities for the final editing of this paper.

## Appendix A. Velocity and attenuation from the reformulated BISQ model

The extension of the BISQ model to transversely isotropic poroelastic media [33] is based on the constitutive equations for anisotropic porous media formulated by [23] in accordance with the homogenisation theory [1,2]. These equations, in the frequency domain with the assumption of $\exp(-j\omega t)$ frequency dependence, are [23] as follows:

$$\tilde{\sigma} = \tilde{c}\tilde{e} - \tilde{\alpha} P, \tag{A.1}$$

$$\sigma_{ij}^{f} = -\phi p \delta_{ij} = \frac{\phi}{\beta}[\tilde{\alpha}\tilde{e} + \phi \nabla \cdot (U - u)]\delta_{ij}, \tag{A.2}$$

$$\frac{\partial \sigma_{ij}}{\partial x_j} = \nabla \cdot \tilde{\sigma} = -\omega^2[\rho_s(1-\phi)u + \phi\rho_f U], \tag{A.3}$$

$$W = \phi(U - u) = -\frac{\tilde{K}(\omega)(\omega^2 \rho_f u - \nabla P)}{j\omega}. \tag{A.4}$$

In these equations, $\tilde{\sigma}$ is the total stress tensor of the saturated porous medium, $\tilde{e}$ the strain tensor of the porous medium, $\tilde{c}$ the solid frame stiffness tensor containing five independent drained elastic coefficients (i.e. $c_{11}, c_{12}, c_{13}, c_{44}$ and $c_{33}$) and $\tilde{K}(\omega)$ is the frequency-dependent generalised Darcy's tensor described by two constant permeability constant. After [5,6,34], the components of this tensor in terms of the complex permeability elements $\kappa_i(\omega)$ for low frequency range is given by

$$K_i(\omega) = \frac{\kappa_i(\omega)}{\eta} = \frac{j\phi}{\omega\rho_f}\left[\frac{\rho_a/\rho_f + \phi}{\phi} + \frac{j\omega_i}{\omega}\right]^{-1}, \tag{A.5}$$

where

$$\frac{\omega_i}{\omega} = \frac{\eta\phi}{\kappa_i \rho_f \omega} \tag{A.6}$$

for $i = 1$ and 2. For isotropic conditions the complex permeability element reduces to

$$K_i(\omega) = K(\omega) = \frac{\kappa(\omega)}{\eta} = \frac{j\phi}{\omega\rho_f}\left[\frac{\rho_a/\rho_f + \phi}{\phi} + \frac{j\omega_c}{\omega}\right]^{-1}, \tag{A.7}$$

where

$$\frac{\omega_c}{\omega} = \frac{\eta\phi}{\kappa\rho_f\omega}, \tag{A.8}$$

The poroelastic coefficients $\alpha$ of the effective stress is given by

$$\alpha = 1 - \frac{K_b}{K_m}. \tag{A.9}$$

The compressibility coefficient, $\beta$, determined under undrained conditions, is given by

$$\beta = \frac{\phi}{K_f} + \frac{\alpha - \phi}{K_m}. \tag{A.10}$$

By considering isotropic conditions, a new partial differential equation for the fluid pressure and the solid frame displacement is obtained from Eqs. (5) and (A.4), after some algebraic development:

$$\theta \nabla^2 P - \left(\frac{\phi}{F}\right) P - \dot{\alpha} \nabla \cdot u = 0, \tag{A.11}$$

where $\theta = -K(\omega)/j\omega$ and $\dot{\alpha} = \alpha_0 + \rho_f \omega^2 \theta$.

Eliminating the fluid displacement vector, $U$, and the total stress tensor, $\tilde{\sigma}$, from Eqs. (A.1), (A.3) and (A.4) and by using Eq. (A.11) one obtains after some algebraic transformations, three partial differential equations associated with the two compressional fast and slow waves and the vertical polarised shear waves:

$$\left[(\lambda+2\mu)\frac{\partial^2}{\partial x^2}+\mu\frac{\partial^2}{\partial z^2}+\omega^2\dot{\rho}\right]u_x+(\lambda+\mu)\frac{\partial^2 u_z}{\partial x\partial z}-\dot{\alpha}\frac{\partial P}{\partial x}=0,$$
$$(\lambda+\mu)\frac{\partial^2 u_x}{\partial x\partial z}+\left[\mu\frac{\partial^2}{\partial x^2}+(\lambda+2\mu)\frac{\partial^2}{\partial z^2}+\omega^2\dot{\rho}\right]u_z-\dot{\alpha}_z\frac{\partial P}{\partial z}=0,$$
$$-\dot{\alpha}\left(\frac{\partial u_x}{\partial x}+\frac{\partial u_z}{\partial z}\right)+\left[\theta\left(\frac{\partial^2}{\partial x^2}+\frac{\partial^2}{\partial z^2}\right)-\frac{\phi}{F}\right]P=0. \tag{A.12}$$

To solve the above system of equations (Eq. (A.12)), a plane harmonic wave of the following form is assumed:

$$(u_x,u_y,u_z,\mathbf{P})=(b_x,b_y,b_z,P)\,\mathrm{e}^{\mathrm{j}(kx+z\xi)}, \tag{A.13}$$

is propagating in the poroelastic porous medium, and proceed as in [33] for the derivation of the phase velocities and attenuations of compressional waves (fast and slow) and the vertical polarised shear wave, by first replacing the poroelastic coefficients by their equivalent for isotropic conditions. These phase velocities and attenuations are derived in the same manner as in [33] except that in Eq. (24a) from [33] the ratio $\bar{\beta}/s$ is replaced by $\phi/F$. For the case where the frequency $\omega$ is much smaller than the Biot's characteristic frequency $\omega_c$, Dvorkin and Nur [11] derived approximate expressions for the velocity and the coefficient of attenuation of the fast compressional waves. Because the principal difference between the models reside in the definition of the Squirt-flow coefficient, similar approximate expressions for the fast compressional wave can be derived by substituting the parameters in the BISQ model by their equivalent in their new model. This gives

$$V_{\mathrm{p1}}=\frac{1}{\mathrm{real}(\sqrt{Y})},\qquad a_1=\omega\,\mathrm{imag}(\sqrt{Y}), \tag{A.14}$$

where

$$Y=\frac{\dot{\rho}}{M+F(\dot{\alpha}_0^2/\phi)}=\frac{\rho+(\omega\rho_{\mathrm{f}})^2\theta}{M+F(((\alpha_0+\omega^2\rho_{\mathrm{f}}\theta)^2)/\phi)},\quad \theta=-\frac{\phi}{\omega^2\rho_{\mathrm{f}}}\left[\frac{\rho_{\mathrm{a}}/\rho_{\mathrm{f}}+\phi}{\phi}+\mathrm{j}\frac{\eta\phi}{\kappa\rho_{\mathrm{f}}\omega}\right], \tag{A.15}$$

where $\dot{\rho}=\rho+(\omega\rho_{\mathrm{f}})^2\theta=(1-\phi)\rho_{\mathrm{m}}+\phi\rho_{\mathrm{f}}+(\omega\rho_{\mathrm{f}})^2\theta$. The inverse of the quality factor $Q^{-1}$ is related to the attenuation coefficient $a$ and the $V_{\mathrm{p1}}$ as

$$Q^{-1}=\frac{2aV_{\mathrm{p1}}}{\omega}. \tag{A.16}$$

In the BISQ model [11], the frequency-dependence of velocity and attenuation is controlled by the Squirt-flow coefficient $F_{\mathrm{sq}}$ in the reformulated BISQ model a frequency-dependent bulk density, $\dot{\rho}$, and poroelastic coefficient, $\dot{\alpha}_0$, were introduced in the same way as in [33].

## References

[1] J.L. Auriault, Dynamic behaviour of porous medium saturated by a Newtonian fluid, Int. J. Eng. Sci. 18 (18) (1988) 775–785.
[2] J.L. Auriault, L. Borne, R. Chambon, Dynamics of porous saturated media, checking of the generalized law of Darcy, J. Acoust. Soc. Am. 77 (1985) 1641–1650.
[3] A.I. Best, C. McCann, J. Southcott, The relationship between the velocities, attenuations and petrophysical properties of reservoir sedimentary rocks, Geophys. Prosp. 42 (1994) 151–178.
[4] A.I. Best, C. McCann, Seismic attenuation and pore fluid viscosity in clay-rich reservoir sandstones, Geophysics 60 (1995) 1386–1397.
[5] M.A. Biot, Theory of propagation of elastic waves in fluid saturated-porous solid. I. low frequency range, II. High frequency range, J. Acoust. Soc. Am. 28 (1956) 168–191.

[6] M.A. Biot, Mechanics of deformation and acoustic propagation in porous media, J. Appl. Phys. 33 (1962) 1482–1498.
[7] F. Birch, The velocity of compressional waves in rocks at 10 kilobars, Part 1, J. Geophys. Res. 65 (1960) 1083–1102.
[8] T. Bourbié, O. Coussy, B. Zinszner, Acoustics of Porous Media, Gulf Publishing, Paris, France, 1987.
[9] M.S. Diallo, E. Appel, Acoustic waves attenuation and velocity dispersion in fluid-filled porous media: theoretical and experimental investigations, Ph.D. Thesis, Eberhard Karls University, Tübingen, 2000.
[10] M.S. Diallo, E. Appel, Acoustic wave propagation in saturated porous media: reformulation of the Biot/Squirt (BISQ) flow theory, J. Appl. Geophys. 44 (2000) 313–325.
[11] J. Dvorkin, A. Nur, Dynamic poroelasticity: a unified model with the Squirt flow and the Biot mechanism, Geophysics 58 (1993) 524–533.
[12] J. Dvorkin, R. Nolen-Hoeksema, A. Nur, The Squirt flow mechanism: macroscopic description, Geophysics 59 (1994) 428–438.
[13] J. Dvorkin, G. Mavko, A. Nur, Squirt flow in fully saturated rocks, Geophysics 60 (1995) 97–107.
[14] J. Dvorkin, A. Nur, C. Chaika, Stress sensitivity of sandstone, Geophysics 61 (1996) 444–455.
[15] M.T. Galdwin, F.D. Stacey, Anelastic degradation of acoustic pulses in rocks, Phys. Earth Planet. Int. 28 (1974) 17–22.
[16] L. Geli, B. Pierre-Yves, D.P. Schmitt, Seismic wave propagation in a very permeable water-saturated surface layer, J. Geophys. Res. 92 (1987) 7931–7944.
[17] G.A. Gist, Fluid effects on velocity and attenuation in sandstones, J. Acoust. Am. 96 (1994) 1158–1173.
[18] B. Gurevich, S.L. Lopatnikov, Velocity and attenuation of elastic waves in finely layered porous rocks, Geophys. J. Int. 121 (1995) 933–947.
[19] D. Han, A. Nur, D. Morgan, Effect of porosity and clay content on wave velocities in sandstones, Geophysics 51 (1986) 2093–2107.
[20] J. Hornung, Dynamische Stratigraphie, Reservoir- und Acquifersedimentologie einer alluvialen Ebene: Der Stubensandstein in Baden-Wurttemberg, Ph.D. Thesis, Eberhard Karls University, Tübingen, 1998.
[21] R. Jaritz, Quantifizierung der Heterogenität einer Sandsteinmatirx, Ph.D. Thesis, Eberhard Karls University, Tübingen, Mittlerer Keuper, Wuttemberg, 1999.
[22] T.D. Jones, Pore fluids and frequency-dependent wave propagation in rocks, Geophysics 51 (1996) 1939–1953.
[23] M.N. Kazi-azoual, G. Bonnet, P. Jouanna, Green's functions in infinite transversely isotropic saturated poroelastic medium, J. Acoust. Soc. Am. 84 (1988) 1883–1890.
[24] T. Klimentos, C. MacCann, Relationships among compressional wave attenuation, porosity, clay content, and permeability in sandstones, Geophysics 55 (1990) 998–1014.
[25] T. Klimentos, The effects of porosity–permeability–clay content on the velocity of compressional waves, Geophysics 56 (1991) 1930–1939.
[26] G.M. Mavko, A. Nur, Wave attenuation in partially saturated rocks, Geophysics 44 (1979) 161–178.
[27] G.M. Mavko, D. Jizba, Estimating grain-scale fluid effects on velocity dispersion in rocks, Geophysics 56 (1991) 1940–1949.
[28] T. Mukerji, G. Mavko, Pore fluid effects on seismic velocity in anisotropic rocks, Geophysics 59 (1994) 233–244.
[29] W.F. Murphy Jr., K.W. Winkler, R.B. Kleinberg, Acoustic relaxation in sedimentary rocks: dependence on grain contacts and fluid saturation, Geophysics 51 (1986) 757–766.
[30] M. Münch, Tomographische Messungen an Bohrkernen, Diplomarbeit, Eberhard Karls University, Tübingen, Germany, 1995.
[31] A. Nur, G. Simmons, The effect of saturation on velocity in low porosity rocks, Earth Planet. Sci. Lett. 7 (1969) 183–193.
[32] R.J. O'Connell, B. Budiansky, Viscoelastic properties of fluid-saturated cracked solids, J. Geophys. Res. 82 (1977) 5719–5736.
[33] J.O. Parra, The transversely isotropic poroelastic wave equation including the Biot and the Squirt mechanisms: theory and application, Geophysics 62 (1997) 309–318.
[34] D.P. Schmitt, Acoustic multipole logging in transversely isotropic poroelastic formations, J. Acoust. Soc. Am. 86 (1989) 2397–2421.
[35] J. Schön, Petrophyisk: Physicalische Eigenschaften von Gestein und Mineralien, Ferdinend Enke Verlag, Stuttgart, 1983.
[36] R. Schütt, Experimentelle und Theoristische Untersuchungen zur Dampfung und Geschwindigkeiten von Kompressions und Scherwellen in Sedimentgesteinen bei Ultraschallfrequenzen, Ph.D. Thesis, Technical University, Berlin, Germany, 1992.
[37] A.S. Shapiro, T. Müller, Seismic signature of permeability in heterogeneous porous media, Geophysics 64 (1999) 99–103.
[38] A.P. Shatilo, C. Sondergeld, C.S. Rai, Ultrasonic attenuation in Glenn Pool rocks, northeastern Oklahoma, Geophysics 63 (1998) 465–478.
[39] R.N. Thurson, A.D. Pierce, Ultrasonic Measurement Methods, Academic Press, New York, 1990.
[40] M.N. Toksöz, D.H. Johnson, A. Timur, Attenuation of seismic waves in dry and saturated rocks. I. Laboratory measurements, Geophysics 44 (1979) 681–690.
[41] Z. Wang, Fundamental of seismic rock physics, Geophysics 66 (2001) 398–412.
[42] K.W. Winkler, T.J. Plona, Technique for measuring ultrasonic velocity and attenuation in rocks under pressure, J. Geophys. Res. 87 (B13) (1982) 10776–10780.
[43] T. Yamamoto, T. Nye, M. Kuru, Porosity, permeability, shear strength: crosswell tomography below an iron foundry, Geophysics 59 (1994) 1530–1541.
[44] T. Yamamoto, T. Nye, M. Kuru, Imaging the permeability of a limestone aquifer by crosswell acoustic tomography, Geophysics 60 (1995) 1634–1645.
[45] G. Yu, K. Vozoff, D.W. Durney, The influence of confining pressure and water saturation on dynamic elastic properties of some Permian coals, Geophysics 58 (1993).